Geothermal Atlas for Africa: from resource mapping to performance indicators

Jan Diederik van Wees*[1,2], Jetze Hofstra[2], Hans Veldkamp[1], Marianne van Unen[1], Fred Beekman[2], Job Mos[1]

[1] TNO

[2] Utrecht University

* Corresponding author: jan_diederik.vanwees@tno.nl

1 Introduction

In this section we describe the method for accessing key resource mapping results from Task 9.1 in LEAP RE Geothermal Atlas of Africa towards different geothermal production scenarios, which are envisaged for Africa for geothermal resources.

2 Geothermal Resource characterization

The resources can be grossly differentiated on potential production temperature (between magmatic and non-magmatic, which can either be produced from the following plays types:

- magmatic
    - Fault/fracture zones
- Sedimentary/basement
    - Sedimentary aquifers
    - Fault/fracture zones

The resource play types relate to different (sub)surface engineering aspects which need to be integrated in the resource fast model, involved lead times as well testing and uncertainty aspects involved.

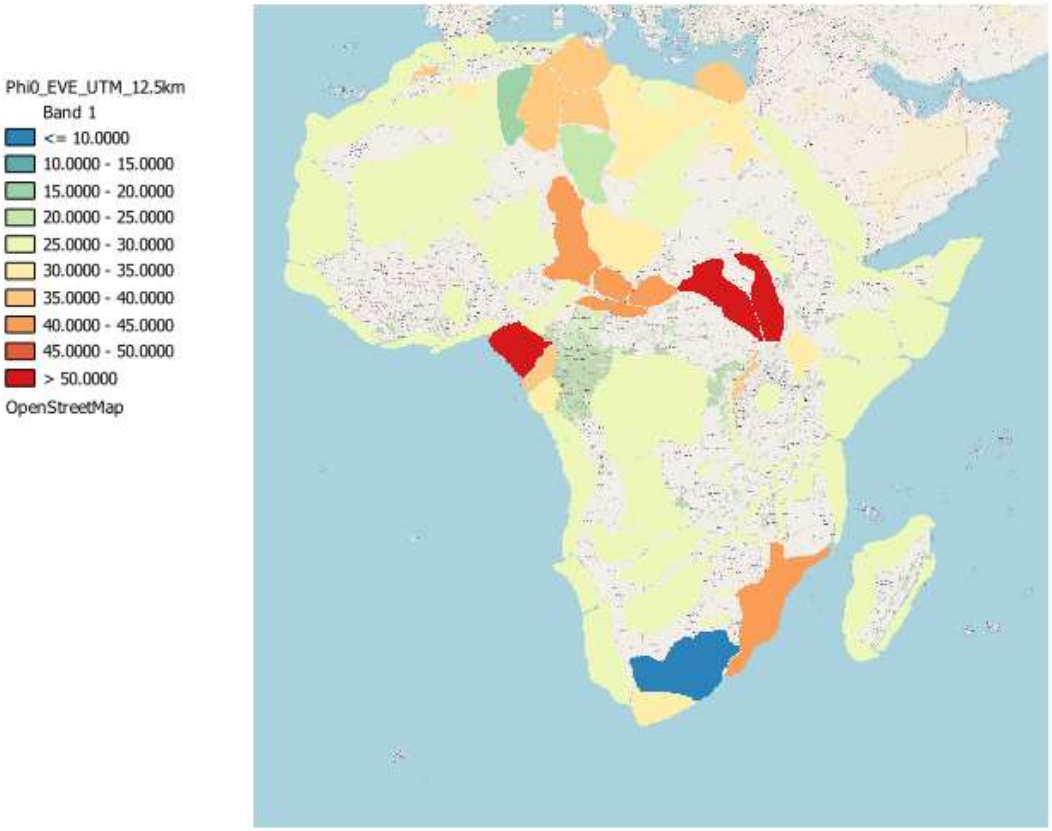

Figure 1 Sedimentary basins (cf Evenick) considered for technical performance assessment in GA4A (coloring according surface porosity ($\varphi_{surface}$) of the basins, determined by Hofstra, 2023) .

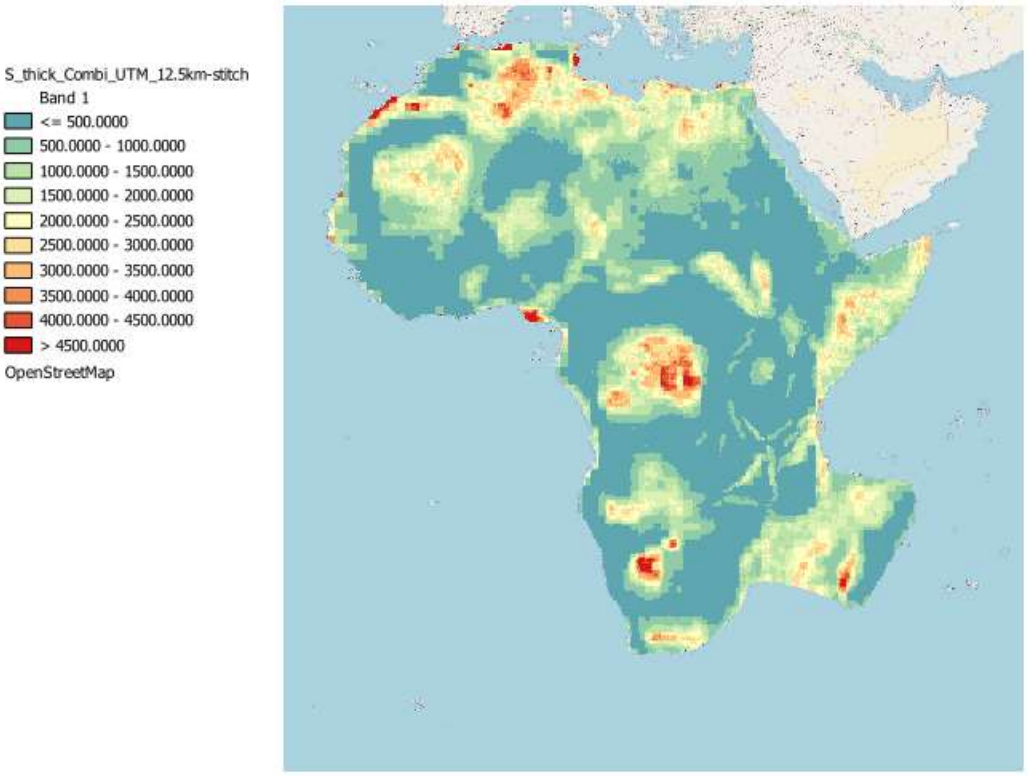

Figure 2 Sedimentary basins thickness from gravity inversion determined by Hofstra (2024) .

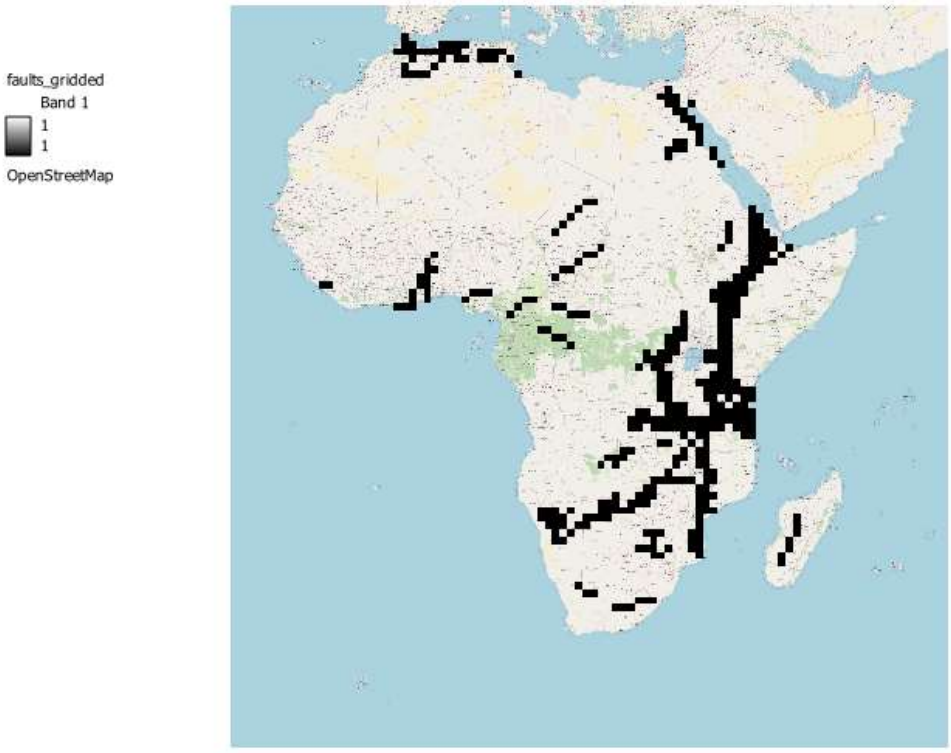

Figure 3 Active fault zone raster discretization based on location of active faults in Africa overlapping the temperature grid resolution in Figure 7

2.1.1 Thermal model

The 3D thermal model was built using a simplified version of a method that was developed for the Netherlands (Bonté et al. 2012, Békési et al 2020). It is based on a lithosphere scale conductive model which includes the sediment thickness, the heat flow, the crustal structure, and the depth of Lithosphere-Asthenosphere Boundary (LAB). For the surface heat flow and underlying grids of the crustal structure LAB, the results of Al-Aghbary et al. (2022) have been used.

The 3D grid measures 8500x8600 kilometer horizontally (85x86 100 km cells), and has a vertical resolution of 250 meter down to 15 kilometer (60 cells), and 2 kilometer down to its base (118 cells).

The surface level ETOPO is used as top reference level. The space between sea level and the bottom of the Madagascar Channel is assigned a separate code to account for the different thermal conditions. Rock (thermal) properties (heat production and thermal conductivity) are assigned to the units using values from Hantschel and Kauerauf (2009). The upper boundary condition is a combination of heat flow and average surface temperature. The lower boundary condition is a temperature of 1200 °C at the LAB. The heat equation is then solved for each vertical stack of grid cells for each grid XY location ("multi-1D thermal calculations"). The resulting grid has a first order estimate of the key properties temperature, heat production and thermal conductivity.
It is acknowledged that the temperature and heat flow conditions in this first model are different where magmatism is present, as reflected by volcanic activity. The known volcanoes were split in two groups: recent (active) ones in the East African Rift area, and old ones in the rest of the continent. In the depth range 3-10 km the heat production was then changed to 4e-5 W/mK for active volcanoes, and 2e-5 W/mK for old volcanoes.

A set of temperature observations from the British Geological Survey (BGS) was used to calibrate the 3D temperature model using ES-MDA (ensemble smoother – multiple data assimilation, Bekesi et al., 2020). This is a heterogeneous data set because in some cases both the depth below surface level and temperature are given, in other cases the depth and the temperature gradient, or only the temperature gradient. This required various processing steps of the data file to make it applicable:

- Recalculate depth as overburden thickness, not with respect to MSL.
- Use the surface temperature grid for the surface temperatures (instead of a fixed Tsurface)
- Temperature observations with gradients lower than 15 °C/km or higher than 45 °C/km are ignored (they appear to be outliers based on a study of the point cloud)
- The gradient is used to calculate the temperature at an (arbitrary) depth of 2500m when no depth is given.
- There is a total of 2243 entries in the database of which 1177 are on the continent. An overburden thickness is given for 296 data points (only in the Algerian Atlas, Algerian Interior Basins, Sirt Basin, Tenere Basin and Tunisian Interior Basins). There are 881 data points without overburden of which 212 appear to be duplicate sets consisting of 1 with and 1 without overburden. After removal of the duplicates 956 temperature observations remain (296 + (881 – 221). If minimum and maximum gradients of 15 and 45 °C/km resp. are adapted, a set of 923 observations remains for the data assimilation.
- For the observation error a linear increase with depth is assumed (0.005 * Z [m)]

The resulting dataset (Figure 4,left) shows considerable clustering in the O&G basins which hampers the data assimilation. Therefore, the data was averaged per model grid cell (right), resulting in an input for the data assimilation consisting of 305 points.

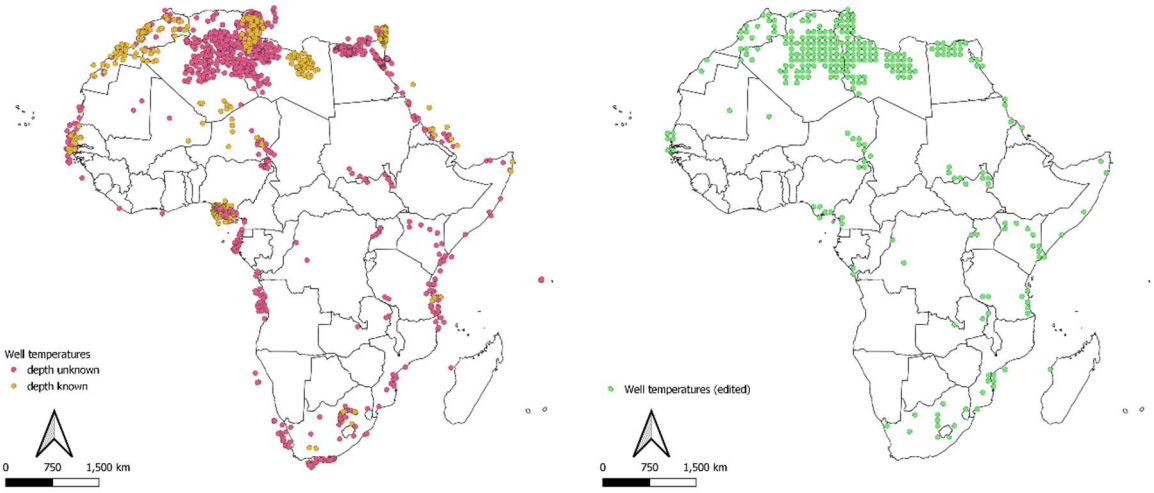

Figure 4 Temperature dataset classified according to depth level (left) and after averaging (right).

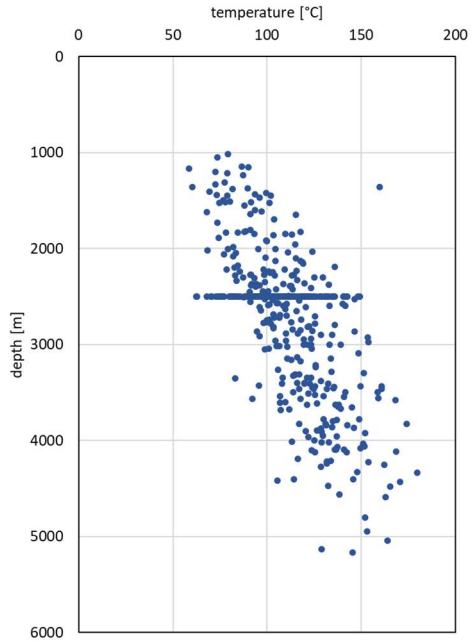

Figure 5 Temperature dataset prior to averaging per model cell. Note data points arbitrarily assigned to 2500m depth.

The resulting dataset was used to update the temperature in the model using an ensemble smoother data assimilation in which the heat production in the crust and in volcanic areas was changed, and the vertical thermal conductivity in the upper part of the model. The results are shown in Figure 6. The scatter of the model points (in orange) around the observations (black line) is a measure of the quality of the model. The results show that the shallow part of the model is slightly too warm (model above observations), and the deep part slightly too cold.

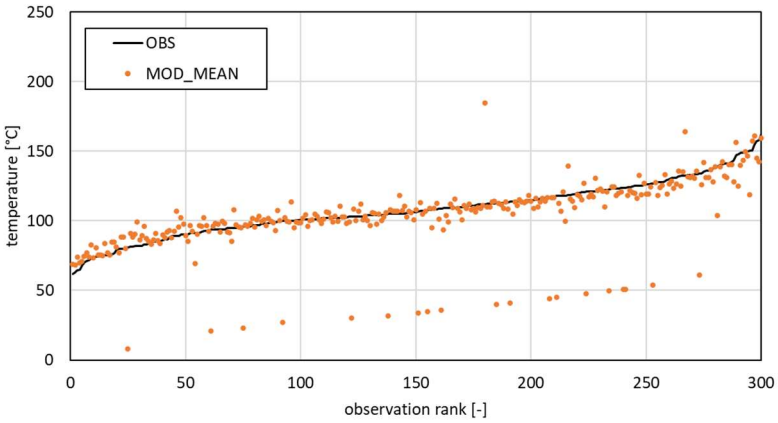

Figure 6 Comparison between temperature observations (black line, sorted on temperature) and model values. Lower outliers are observations located outside the model grid, mostly along the coast.

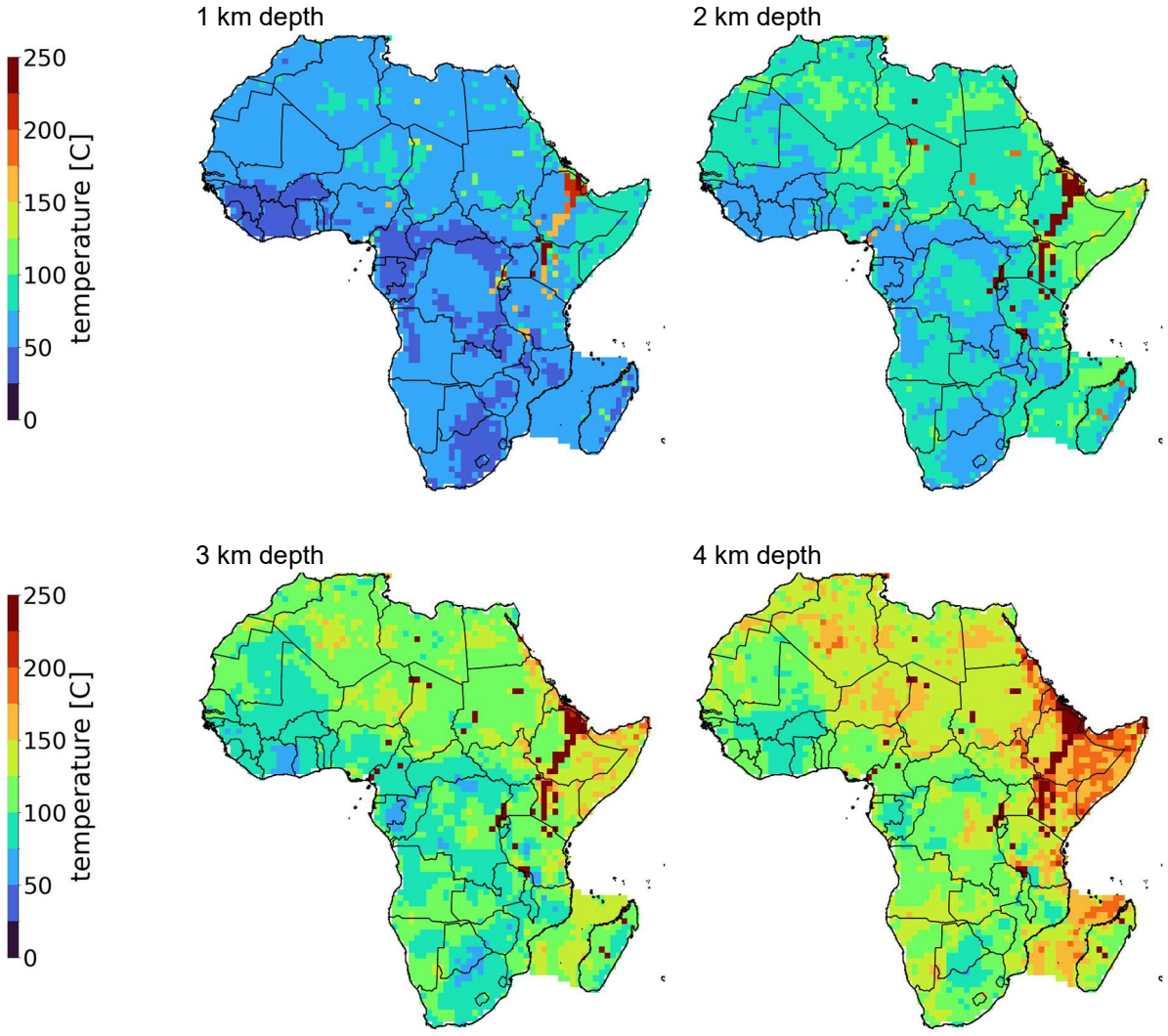

Figure 7 Temperatures at 1,2,3,4 km depth from surface form the 3D temperature model. Magmatic areas have been treated as loci of elevated heat production at a depth range of 3 to 8 km and result in temperatures exceeding 200 °C at 2 km depth.

2.1.2 *Sedimentary reservoirs porosity depth relationship, permeability and potential hydraulic transmissivity*

For the sedimentary basins in GA4A we adopt the basin structures and basin porosity (φ) -depth curves as determined by Hofstra, 2023,2024.

The sedimentary basin porosity-depth are characterized by Athy's relationship:

Equation 1 $$\varphi(z) = \varphi_{base} + (\varphi_{surface} - \varphi_{base}) \cdot e^{-k_{athy} z}$$

Where $\varphi_{surface}$, φ_{base} are surface and base (minimum) porosity, k_{athy} is athy's constant and z is depth in km. $\varphi_{surface}$, φ_{base} and k_{athy} are given in Figure 1, Figure 8 and Figure 9.

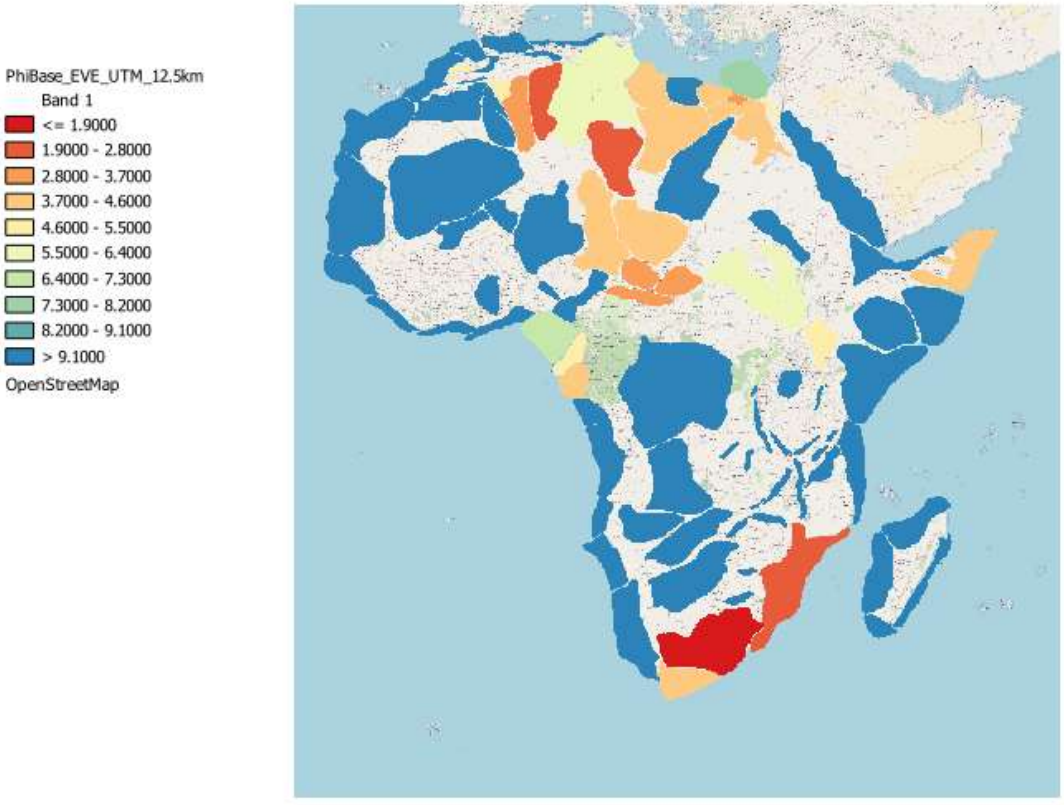

Figure 8 φ_{base} of sedimentary basins (cf Evenick) considered for technical performance assessment in GA4A (Hofstra, 2023) .

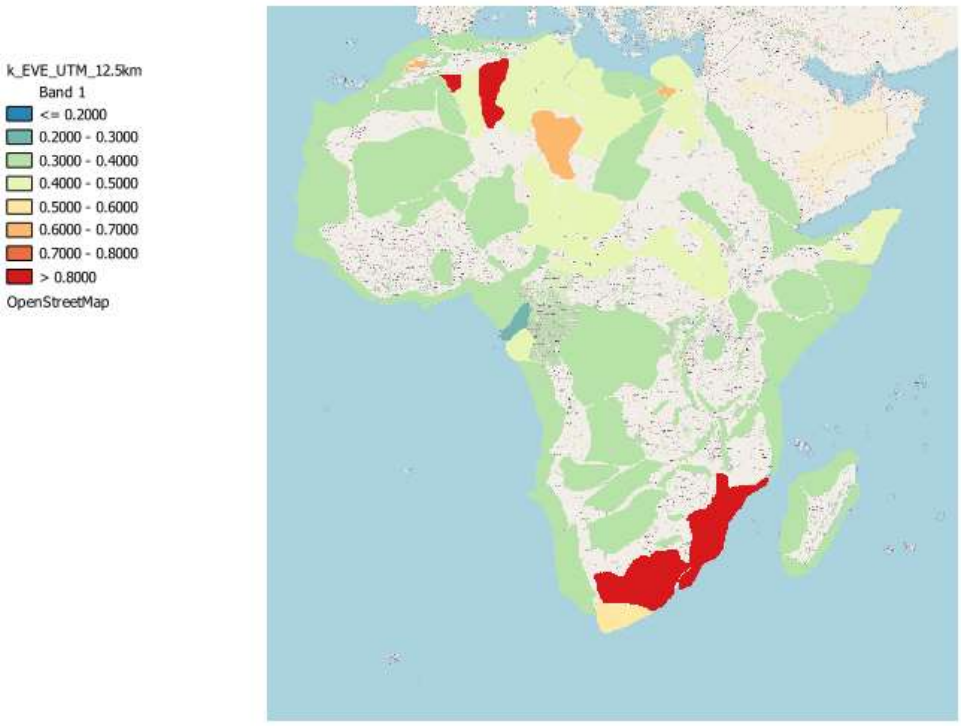

Figure 9 k_{athv} of sedimentary basins (cf Evenick) considered for technical performance assessment in GA4A (Hofstra, 2023).

The depth dependent porosity values have been used to calculate the aquifer permeability k:

Equation 2 $$\ln(k) = a \cdot \varphi^2 + b \cdot \varphi + c$$

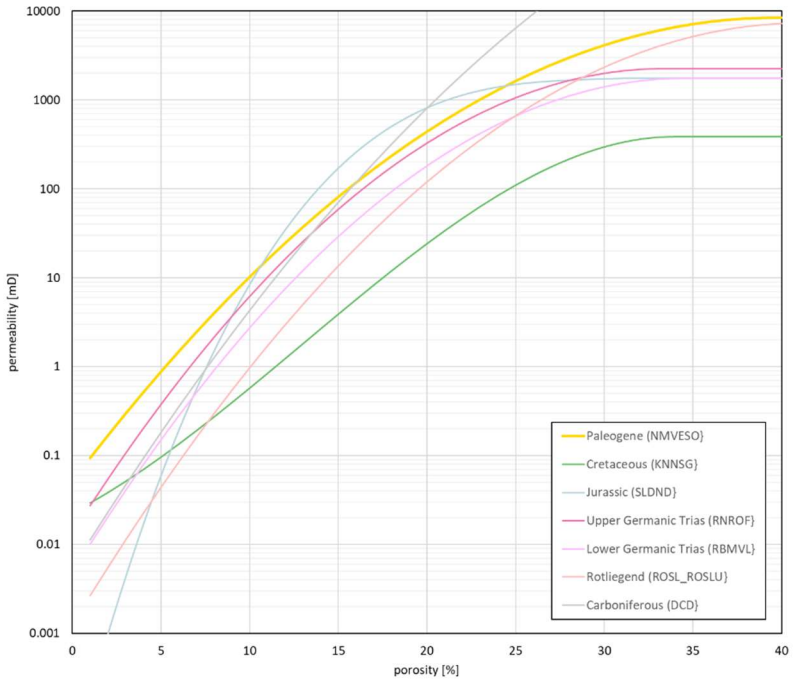

Figure 10 Porosity-permeability relationship for different clastic aquifers in the Netherlands in agreement with Equation 2 (cf ThermoGIS.nl). For GA4A we adopt, a=-0.0092, b= 0.76, c=-6.7, for φ expressed as percentage. corresponding to the Rotliegend formation. The permeability has been truncated for permeabilties in excess of 2500mD.

For a potential aquifer in the sedimentary basins a thickness of 100 m has been assumed.

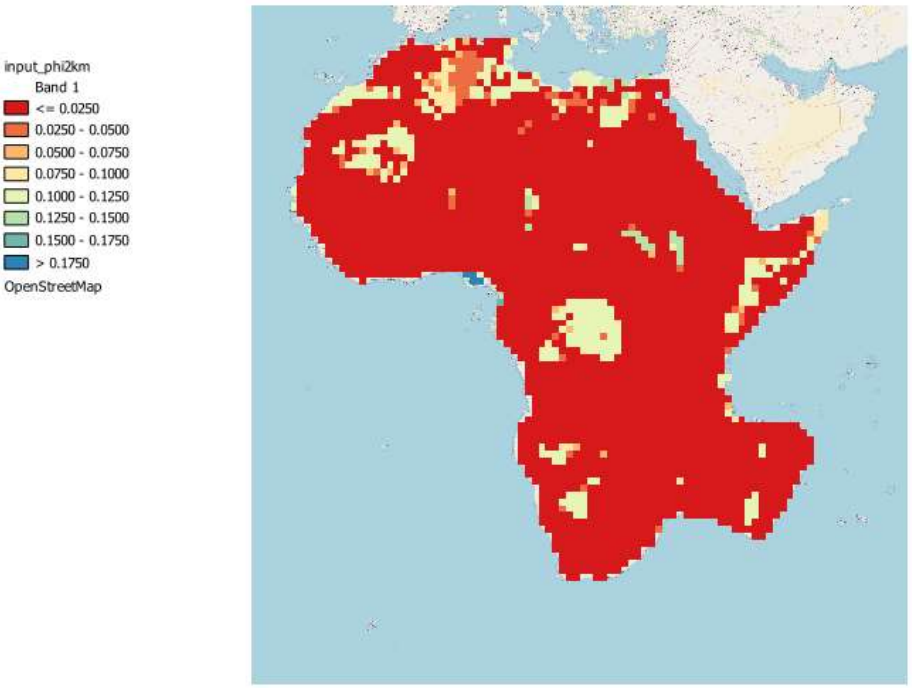

Figure 11 Sedimentary porosity (top) and at 2 km depth.

2.1.3 Fault zone permeability

For active fault zones we assume that fault/fracture permeabity can account for a hydraulic transmissivity of 20Dm up to a depth of 3 km. Corresponding “aquifer” permeability has been set to 10,000 mDarcy and a thickness of 20 m

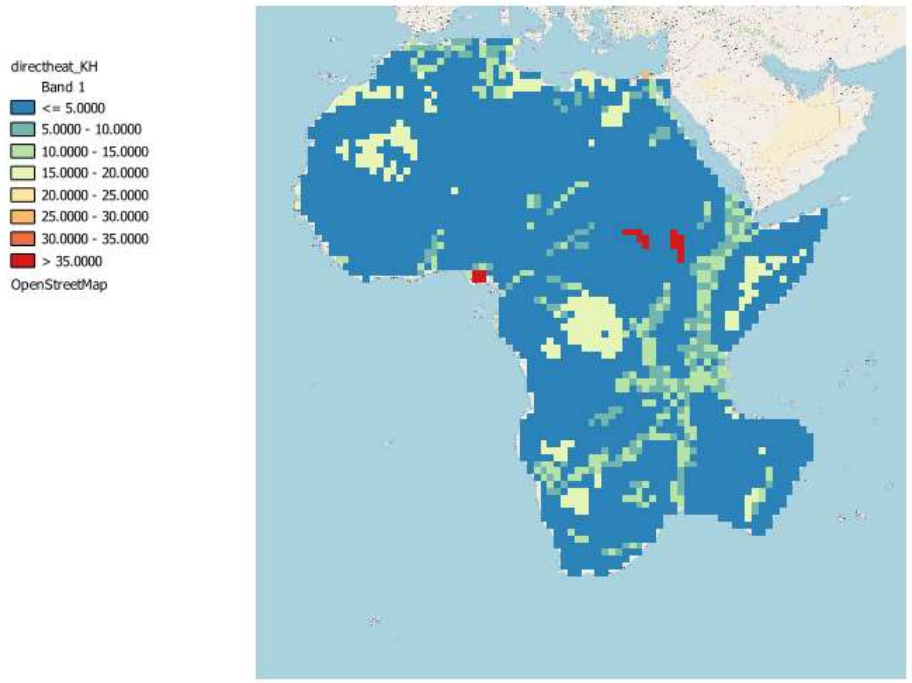

Figure 12 Best of sedimentary and fault transmissivity at 2 km depth.

3 Geothermal Performance model

In GA4A the considered subsurface production system for sedimentary aquifers and fracture aquifers is a doublet system (at least one production and injection well, to provide pressure support).The doublet performance calculations are perfomed with Doubletcalc1D (see section 2), which is a public domain tool (Van Wees et al., 2012, section 3.1). The technical parameters for geothermal doublets are based on industrial standards followed in the Netherlands over the past 15 years which have resulted in over 25 successful geothermal plants (see nlog.nl, ThermoGIS.nl, geothermie.nl and more details are in the references listed in this report). The techno-economic parametrization as detailed in www.ThermoGIS.nl is adopted here, with major modifications for the extension of geothermal energy conversion in order to include chill and Power.

The geothermal power which can be produced takes into account the production flow rate Q, the cooling of the produced brine in the heat conversion process ΔT and the efficiency η of the heat conversion process:

Equation 3 $$E = \eta\ Q\ C\ \Delta T$$

With:

E converted power [W]
η conversion efficiency [-]
C volumetric heat capacity of the brine or circulation fluid (in the Eavor Loop) [J m^{-3} K^{-1}]
ΔT temperature difference between producer and injector at the topside at the heat exchanger [°K].

The conversion efficiency η depend strongly on the application. In this document we include the following heat conversion systems/options which are considered suitable for heat conversion,

- Direct heating with and without Heat Pump
- Adsorption/absorption chiller
- Organic Rankine Cycle or ORC for power

3.1 Resource fast model

3.1.1 Sedimentary aquifers

Geothermal energy production in a doublet system is marked by a producer and injector well, forming a closed loop for the produced brines, which are fully reinjected. At the top side a heat exchanger allows to extract geothermal energy which can be used for direct heating or absorption cooling, or may be converted to electricity. The re-injection assures that during production, pressure support is maintained in the aquifer. The flow at reservoir level can be approximated by a simple equation (Van Wees et al., 2012):

Equation 4 $$Q = \Delta p \frac{\pi\ kH}{\mu\left(ln\left(\frac{L}{r_w}\right)+S\right)}$$

With:

Q flow rate [m^3/s]
Δp pressure difference between injector and producer to drive the flow in the reservoir [Pa]
k permeability [m^2]
H aquifer thickness [m]
μ viscosity [Pa·s]
L distance between injector and producer [m]
r_w well radius [m]
S skin factor [-].

In general, flow rates in the wells are relatively high such that thermal losses are no more that 1-2ºC along the wellbore, when reaching the top-side. The distance between the well perforations at the aquifer depth should be chosen such that the produced waters are marked by a decline in temperature which are preferably negligible during the economic lifetime of the doublet.

The brine production involves Electrical Submersible Pumps (ESP) for production and reinjection of the fluids, with efficiency of $ESP_{n.}$ and the parasitic power needed in the heat conversion process:

Equation 5 $$E_{consup} = Q \frac{\Delta p}{ESPn.}$$

Where Δp is the pressure for driving the thermal loop.

The lead times for design and constructing, testing a doublet system are in the order of months and days respectively

The cost items regarding well construction, completion, and testing are assumed to result in an average total costs of the wells with a quadratic function of True Vertical Depth (TVD)of the reservoir and is given by the following relation:

Equation 6 $$\text{capex}_{\text{wells}} = 375{,}000 + 1050 \cdot s_{curve} \cdot z_{tvdtop} + 0.3 \cdot s_{curve} \cdot {z_{tvdtop}}^2$$

where $\text{capex}_{\text{wells}}$ is the average cost of the well in US$ and z_{tvdtop} is the TVD of the top of the reservoir in meters measured from surface. s_{curve} is curvature factor to correct

In addition to the costs for the wells, costs for an ESP pump needs to be included which is estimated at 0.5 mln $. A single ESP is considered sufficient to drive the thermal loop.

3.1.2 Geothermal doublet in fault/fractured basement/sediments

Same as doublet, but representing the fractured/fault zone as a thin reservoir. The resource fast model may need to take into account potential cooling over time of production temperatures in case of reinjection of fluids. In the current implementation this is neglected

3.1.3 Magmatic vs non-magmatic resources

The same resource fast model can be used for magmatic resources, however in many cases the wells are self flowing (due to natural lift). In addition the number of injection wells can be considerably lower than for non-magmatic settings as pressure support is less important thanks to natural recharge. In addition the production temperature may be marked by progressive cooling. All these effects have been considered beyond the scope of this study.

3.2 Energy conversion

3.2.1 Heat conversion -direct heat

For usage of the heat in direct approach it assumed that minimum production temperature is at least 60 °C. Reinjection temperature is set to 40 °C.

Alternatively a heat pump scenario can be used which can produce from geothermal production temperatures from 40 °C, which are heated with the heatpump to 80 °C. The reinjection temperature is set to the production temperature minus 200 °C, with a minimum of 15 °C.

3.2.2 Heat conversion - Chiller

Adsorption or Absorption Chillers can convert low grade heat to chill, with natural refrigerants such as Ammonia or Lithium-Bromide (absorption) or silica gel, zeolite or carbon based materials(adsorption) (Ayou and Coronas, 2020; El-Sharkawy et al., 2014, **Error! Reference source not found.**).

In this study we adopt for chill an $\eta \approx 0.4$ (El-Sharkawy et al., 2014; Ayou and Coronas, 2020).

For chilling we assume the ΔT is strongly limited by the return temperature of the heat conversion process which must be a couple of tens of degrees higher than the ambient temperature which can range up to ca 50°C in summer. In this study we adopt 60 °C as reinjection temperature in the heat conversion, in line with assumptions for solar assisted chillers (El-Sharkawy et al., 2014; Ayou and Coronas, 2020), for minimum production temperature we assume 70 °C .

The parasitic power consumption $E_{conspara}$ for the chiller relates to circulation pumps and the cooling tower:

Equation 7 $$E_{conspara} = e_{para} E$$

Where e_{para} is the parasitic power consumption as fraction of the chilling power E. e_{para} is typically about 0.1 (Ayou and Coronas, 2020; El-Sharkawy et al., 2014)

The investment costs of chiller in the market are estimated around 800-1000 US$/kW chilling capacity at capacity values exceeding 100 Refrigeration Tons (RT). One RT is equivalent to 3.52 kW. These values are based on cost estimates from DOE (2017).

In addition geothermal brines require a heat exchanger which can sustain high salinity. Costs for heat exchanger are estimated at 100US$/kW chill capacity. This estimate is based on Dutch heat exchanger cost for gross power which is about 35 US$/kW gross, corrected for gross to net conversion.

The expected lead times are in the order of months to a year.

3.2.3 ORC and power production

For power production with a binary cycle (Organic Rankine Cycle or ORC, **Error! Reference source not found.**) the efficiency is strongly temperature dependent, somewhere in the range of $\eta \approx 0.05 - 0.15$ for aquifer temperatures of 80-150°C. The actual efficiency and temperature range which can be effectively be used depend on the ambient temperature and cooling source (Moon and Zarrouk, 2012).The net efficiency for the ORC as function of production temperature used in this study corresponds to:

Equation 8 $$\eta = 0.6\ (T_{prod} - T_s) / (T_{prod} + T_s + 2\ x\ 273)$$

Where T_{prod} and T_s are production and yearly average surface temperature.

Application of ORC systems for existing oil wells with high water cut has been demonstrated in Europe in the H2020 funded project MEET (www.meet-h2020.com), and has been proposed in various studies for enhancing RE power generation at existing hydrocarbon producing facilities (i.e. Aulds et al., 2014).

3.3 Raster analysis

The ThermoGIS analysis methodology has been used (Van Wees et al., 2012, Vrijlandt et al., 2020; ThermoGIS.nl). At each location in the region of interest the ThermoGIS workflow calculates the techno-economic performance of the doublet system in an automatic way for aquifer input parameters on k, H, reservoir temperature, including optimization of a number of engineering parameters to enhance geothermal energy production. This calculation model for the doublet system is performed by the public domain tool of TNO called DoubletCalc1D (Van Wees et al., 2012; www.nlog.nl/tools), which includes also frictional and thermal losses along the well bores. It adopts both map derived aquifer specific values as well as constant values for doublet parameters as listed in Table 1. Some parameters of DoubletCalc1D (including viscosity as a function of temperature and salinity) are described in more detail in Van Wees et al. (2012) and the online documentation of ThermoGIS (www.ThermoGIS.nl). The depth dependent salinity *s* (ppm) is based on the following equation:

Equation 9 $$s = \left(s_0 + s_{grad}\,(z + 0.5H)\right)$$

Where *z* is top depth and *H* thickness of the aquifer, both in m. In the Netherlands aquifers with salinities up to 180,000 ppm do not give any problems in production.

The Skin factor of -1 corresponds to having a 45° slanted well in the reservoir and the -3 corresponds to the situation after well stimulation (hydraulic or acidication)

3.3.1 Incorporation of subsurface uncertainties

The workflow allows for the assessment of the effects of uncertainty in the two parameters with the largest variation and most significant impact on the geothermal power: permeability and thickness. Using the standard deviation maps for these two parameters and the stochastic ThermoGIS workflow, expectations curves can be generated as a function of uncertainty of subsurface parameters (**Error! Reference source not found.**). These can also be presented in map view (e.g. P10, P50 and P90 maps).

Two of the parameters are optimized per location, per reservoir: the distance between the wells and the pumping pressure. A well distance which is too small will cause thermal breakthrough of reinjected cold water in the production well. On the other hand, a too large distance will increase the risk of not having pressure connection between the wells. The pumping pressure should be large enough to achieve good flow rates, but not unnecessarily high to avoid the risk of seismic events and to avoid high electricity costs to drive the pump. Both the optimal well distance and pump pressure vary dependent on the subsurface conditions.

The well distance is optimized in such a way that the maximum cooling of the production water is 1% of ΔT after 50 years. This means that the difference between production water and return (injection) temperature after 50 years, is at least 99% of the original temperature difference.

The optimal pump pressure is obtained by minimizing the Levelized Cost of Energy (LCOE), with the constraint that the maximum pressure difference in the loop for driving the water flow as is not exceeding about 30% above hydrostatic pressure, to avoid risks for endangering well integrity in the injector well and to avoid induced seismicity. In order to minimize the unit technical costs, the economic model needs to be run as well, performing a cost-benefit analysis, as detailed further below.

Table 1 Technical parameters aquifers and fault zones

Technical parameter	symbol	value	unit
Aquifer/fault top depth	z	varies	m
Aquifer/fault thickness	H	100/1	m
aquifer net-to-gross	Ng	1	-
aquifer permeability	k	Equation 6	millidarcy
aquifer temperature	Tprod	temperature model at z+0.5H	°C
aquifer water salinity	s	Equation 9	ppm
aquifer water salinity at z=0	s_0	0	ppm
aquifer water salinity gradient	s_{grad}	47	Ppm/m
aquifer kh/kv ratio	Kh/v	1	-
return temperature ($\Delta T \approx T_{prod} - T_{inj}$)	Tinj	Application dependent	°C
Conversion efficiency	η	Application dependent	
Parasitic power needs for conversion process (fraction of net power)	e_{para}	Application dependent	
minimum aquifer temperature	Tmin	Application dependent (40-80C)	°C
distance between the two wells	L	optimized	m
pump system efficiency	ESPn	0.6	-
production pump depth	ESPz	500	m
pump pressure, limited to 30% of hydrostatic pressure	ΔPtotal	optimized	bar
well trajectory curvature factor	s_{curve}	1.1	-
calculation segment length	Δz	50	m
inner diameter (casing)	rw	8.5	inch
casing roughness	m	1.38	milli-inch
injector well skin (with stimulation)	S	-1 (-3)	-
production well skin (with stimulation)	S	-1 (-3)	-

3.4 Techno-Economic Performance calculation

The ThermoGIS economic model is based on a cashflow calculation which determines the levelized costs of energy, US$ct/RTh (for chill), US$ct/kWh and NPV (million US$). The economic model takes as input the gross power outcome of the DoubletCalc calculation and converts this to net power, in agreement with either the direct heat, heat pump, Chiller or ORC scenario as described above. The subsurface setting of the reservoir, pumping power requirements, production parameters and net power produced are used to determine the CAPEX and OPEX for the lifetime of the project.

The cost engineering parameters for the cashflow calculations are corresponding

- Generic economic parameters (Table 2)
- Subsurface cost parameters (Table 3)
- Direct Heat cost parameters including heat exchanger for brines (Table 4 Cost-engineering parameters for the direct heat scenario in the discounted cashflow calculations

Economic parameter	symbol	value	unit
annual load hours	Hload	5000	hour
Capex Base expense	CAPEXbase	3	million US$
Capex Variable (including heat exchanger)	CAPEXother,var	300	US$/kW
base opex	OPEXbase	0	kUS$
annual opex per unit power	OPEXpower	50	US$/kW
Additional opex per unit heat	OPEXheat, var	0.19	US$ct/kWh

Table 5 Cost-engineering parameters for the direct heat with heat pump scenario in the discounted cashflow calculations, in addition to the parameters in Table 4.

Economic parameter	symbol	value	unit
annual load hours	Hload	5000	hour
Heat Pump Capex Variable	CAPEXhp, var	600	US$/kW
Annual heat pump opex per unit power	OPEXpower	10	US$/kW

- Table 6)
- Direct heat with heat pump parameters (Table 5)
- Chiller cost parameters including heat exchanger for brines (Table 6)
- ORC cost parameters including heat exchanger for brines (Table 7)

Table 2 General cost-engineering parameters for calculations.

Economic parameter	symbol	value	unit
economic lifetime	Teconomic	15	year
Drilling & construction time (drill & test)	Tdrilling_construction	1	year
electricity price for operations	Celectricity	8	US$ct/kWh
tax rate	Ptax	20	%
interest on loan	Pinterest	5	%
inflation	Pinflation	2	%
required return on equity	Preturnonequity	15	%
debt ratio	Pdebtratio	80	%
Contingency (on all CAPEX)	Pcontingency	15	%

Table 3 Cost-engineering parameters for the subsurface engineering used in the discounted cashflow calculations.

Economic parameter	symbol	value	unit
Capex of each well	CAPEXwells	Equation 6	US$
capex of each well stimulation (per well), if stimulated	CAPEXstimulation	0.75	million US$

Table 4 Cost-engineering parameters for the direct heat scenario in the discounted cashflow calculations

Economic parameter	symbol	value	unit
annual load hours	Hload	5000	hour
Capex Base expense	CAPEXbase	3	million US$
Capex Variable (including heat exchanger)	CAPEXother,var	300	US$/kW
base opex	OPEXbase	0	kUS$
annual opex per unit power	OPEXpower	50	US$/kW
Additional opex per unit heat	OPEXheat, var	0.19	US$ct/kWh

Table 5 Cost-engineering parameters for the direct heat with heat pump scenario in the discounted cashflow calculations, in addition to the parameters in Table 4.

Economic parameter	symbol	value	unit
annual load hours	Hload	5000	hour
Heat Pump Capex Variable	CAPEXhp, var	600	US$/kW
Annual heat pump opex per unit power	OPEXpower	10	US$/kW

Table 6 Cost-engineering parameters for the chiller scenario in the discounted cashflow calculations.

Economic parameter	symbol	value	unit
annual load hours	Hload	5000	hour
Capex Base expense	CAPEXbase	0.5	million US$
Capex Variable (including heat exchanger)	CAPEXother,var	1100	US$/kW
base opex	OPEXbase	10	kUS$
annual opex per unit power	OPEXpower	50	US$/kW

Table 7 Cost-engineering parameters for the ORC scenario in the discounted cashflow calculations.

Economic parameter	symbol	value	unit
annual load hours	Hload	8000	hour
Capex Base expense	CAPEXbase	0	million US$
Capex base expense (connection to grid)	CAPEXother,base	function	US$
Capex Variable (including heat exchanger)	CAPEXother,var	2300	US$/kW
base opex	OPEXbase	10	kUS$
annual opex per unit power	OPEXpower	50	US$/kW

4 Results for energy conversion scenarios

The resulting potential has been calculated by locating at each x,y location the optimal depth for the potential aquifer to being produced, at a resolution of ca 25 km. It produces seven key performance indicator maps as listed in Table 8.

Table 8 Key performance parameters

parameter	**Property name**	**Unit**
Optimized depth of the aquifer	MIDDEPTH	Meter
Temperature at the optimized depth	TEMPRES	°C
transmissivity	KH	Darcy meter
Doublet well distance	L	M
Doublet Production flow rate	FLOWRATE	m3/h
Pressure needed to drive pumps	DP	Bar
Doublet net Production	HPROD	MW
Coefficient of Peformance net production	COP	-
Levelized Costs of Energy	UTC	US$ct/kWh

The potential maps of the base case represent an expected value for potential (p50). In order to illustrate the potential upside we also consider variation in subsurface parameter which results in a more positive business case outcome. So in total the based case complemented with two more positive scenarios have been considered:

- *Basecase:* default flow and thermal properties
- *Flow Upside:* P25 flow properties, based on a lognormal distribution for permeability, which standard deviation of 1 (for the natural logarithm)
- *Thermal upside + Flow upside:* As flow upside with 30% increase of the geothermal gradient in the temperature model

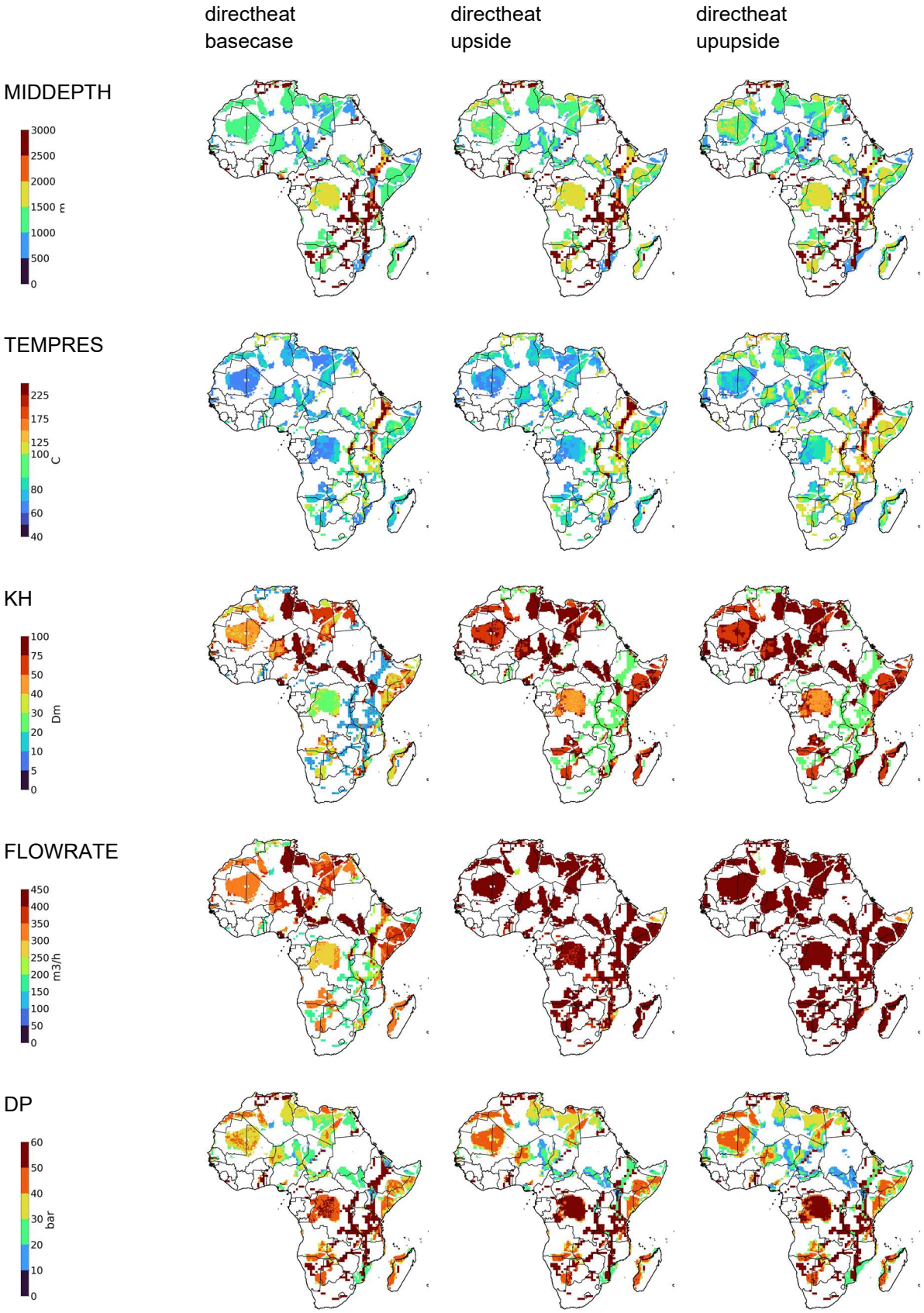
directheat basecase
directheat upside
directheat upupside
MIDDEPTH
3000
2500
2000
1500
1000
500
0
m
TEMPRES
225
175
125
100
80
60
40
C
KH
100
75
50
40
30
20
10
5
0
Dm
FLOWRATE
450
400
350
300
250
200
150
100
50
0
m3/h
DP
60
50
40
30
20
10
0
bar

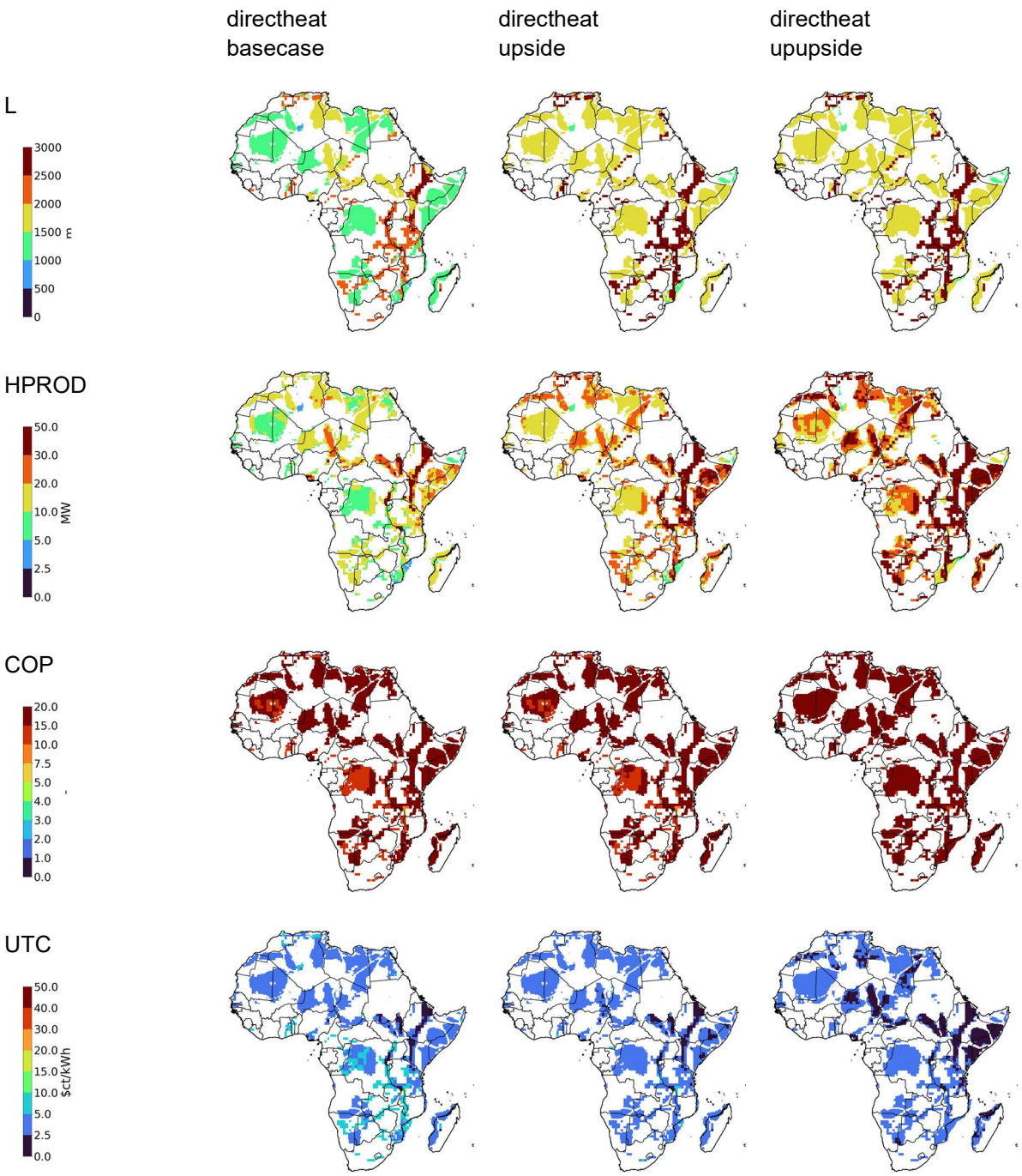

Figure 13 key performance parameters for direct heat production

directheatHP basecase

directheatHP upside

directheatHP upupside

MIDDEPTH

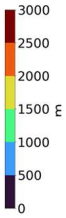

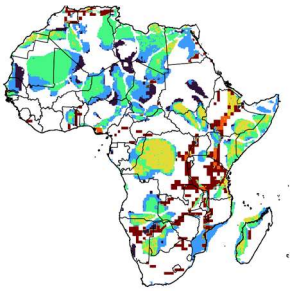

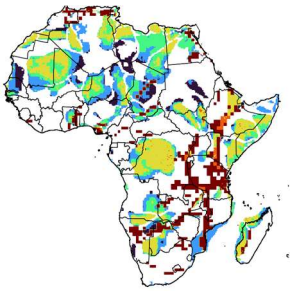

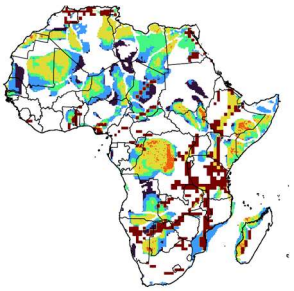

TEMPRES

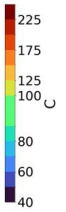

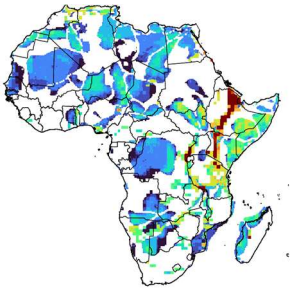

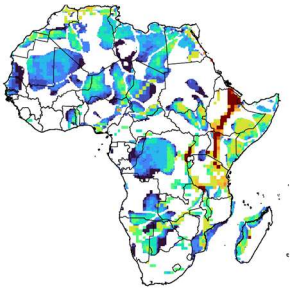

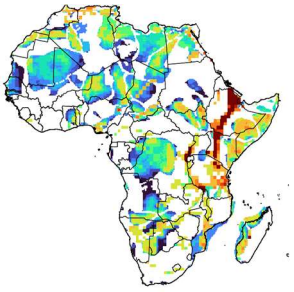

KH

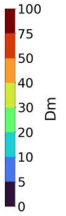

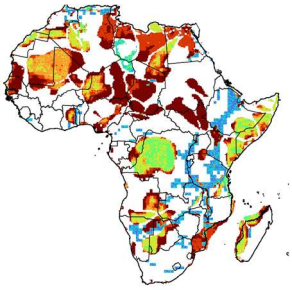

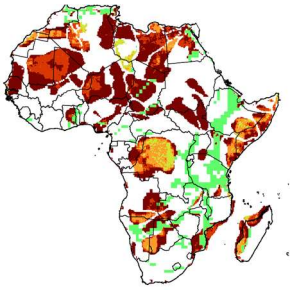

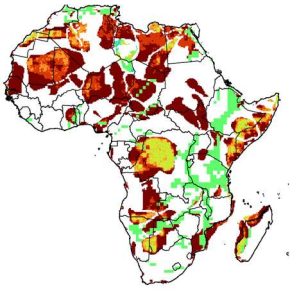

FLOWRATE

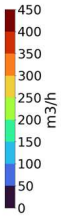

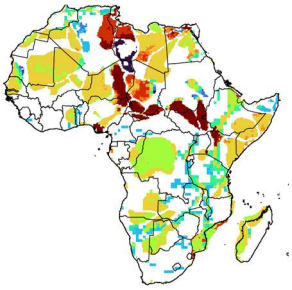

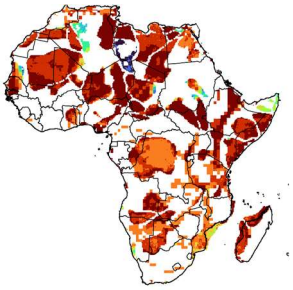

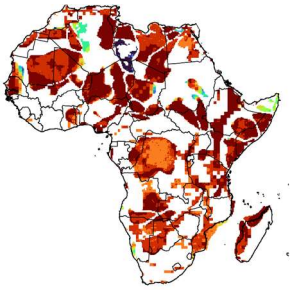

DP

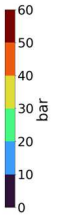

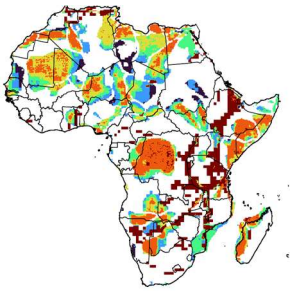

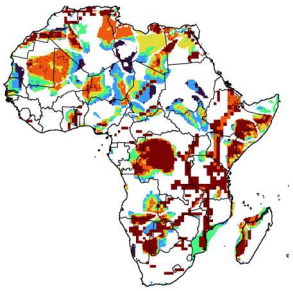

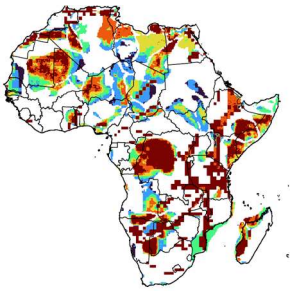

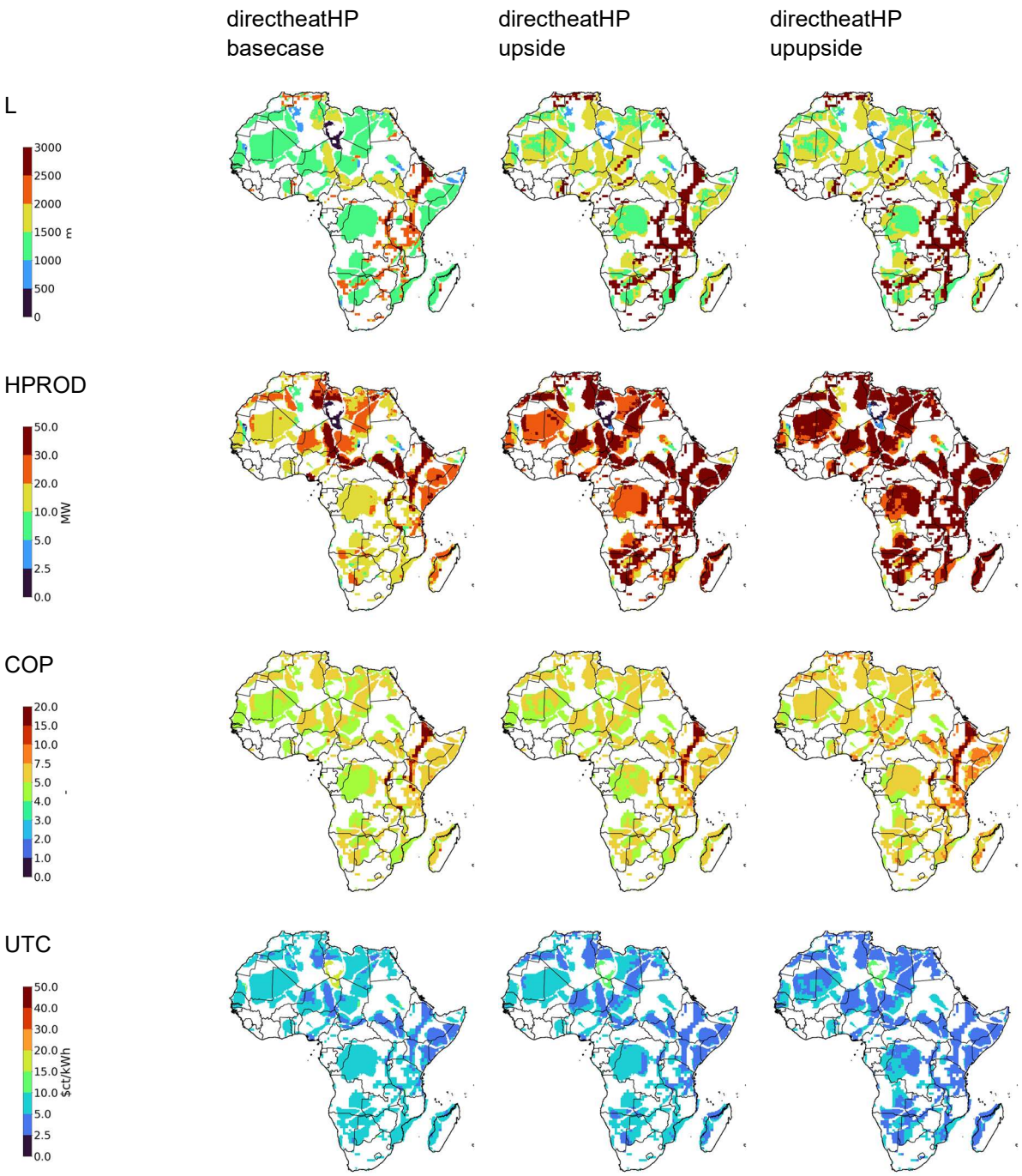

Figure 14 key performance parameters for direct heat production combined with an industrial heat pump

chiller basecase

chiller upside

chiller upupside

MIDDEPTH

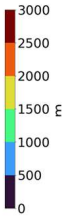

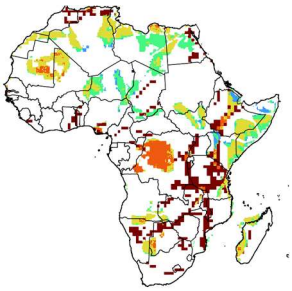

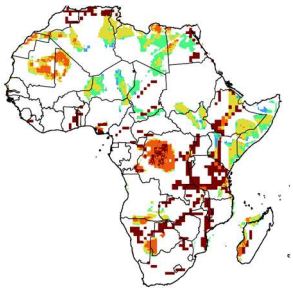

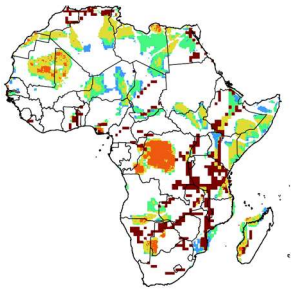

TEMPRES

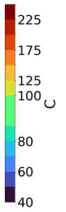

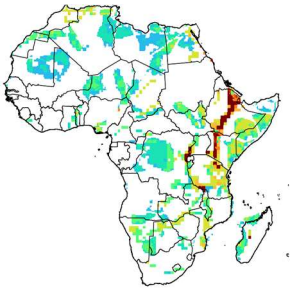

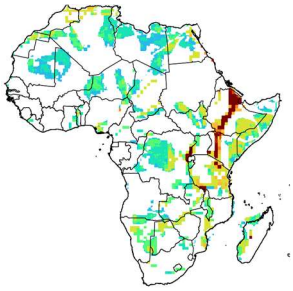

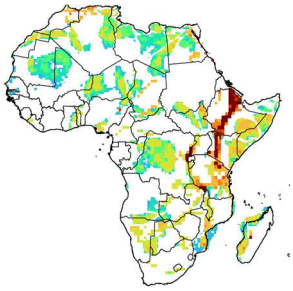

KH

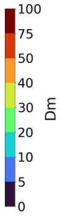

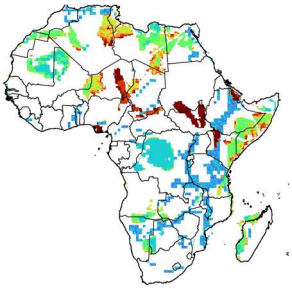

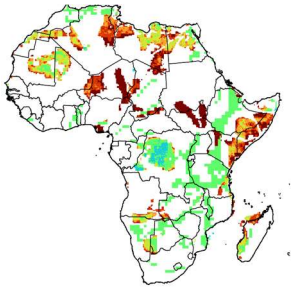

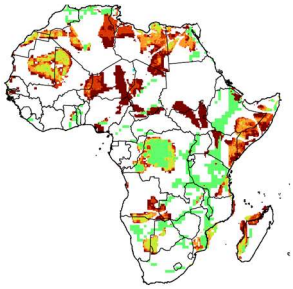

FLOWRATE

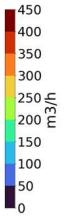

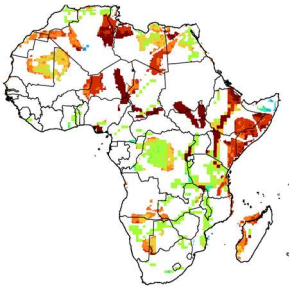

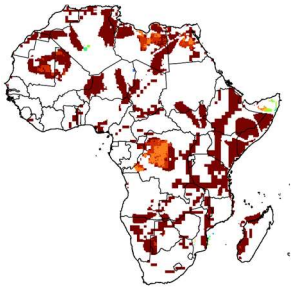

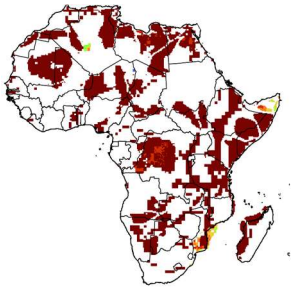

DP

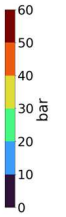

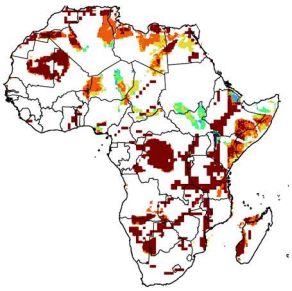

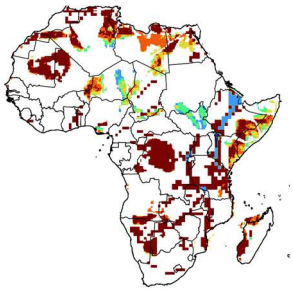

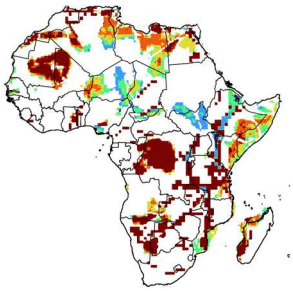

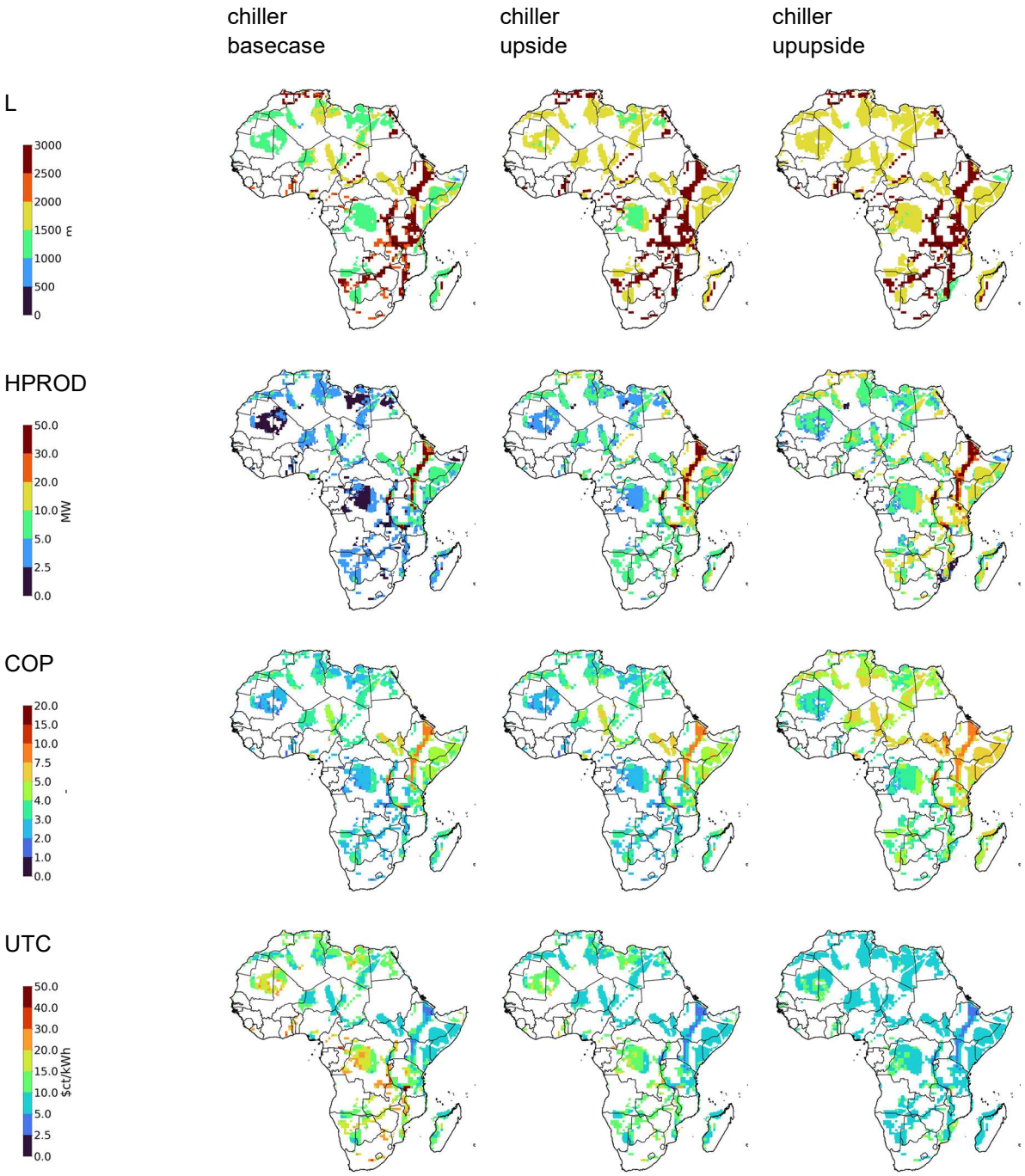

Figure 15 key performance parameters for chiller

ORC basecase

ORC upside

ORC upupside

MIDDEPTH

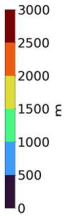

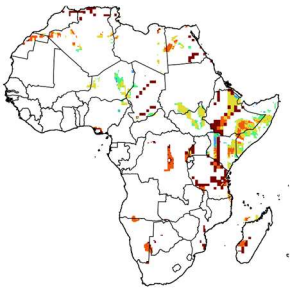

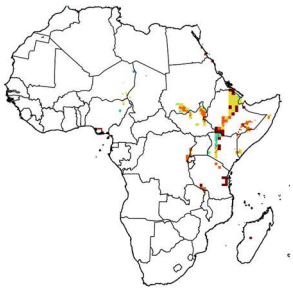

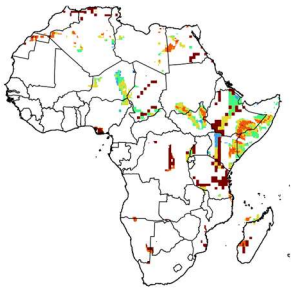

TEMPRES

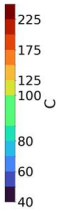

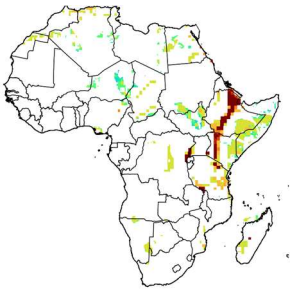

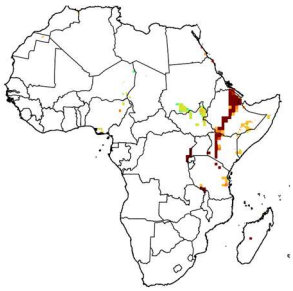

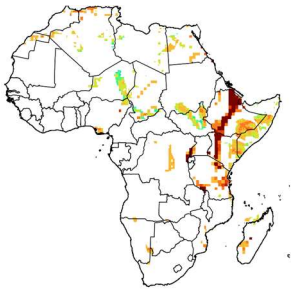

KH

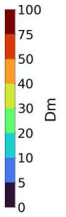

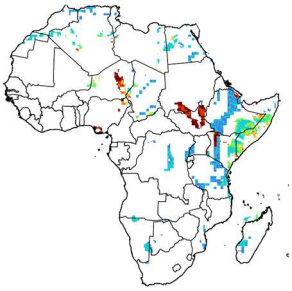

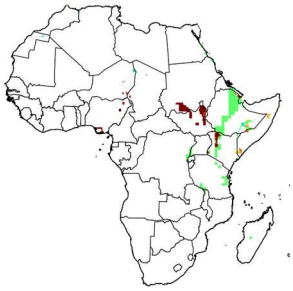

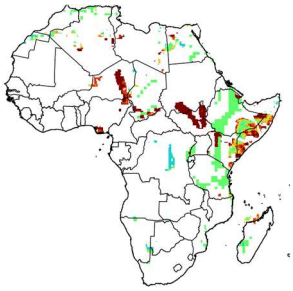

FLOWRATE

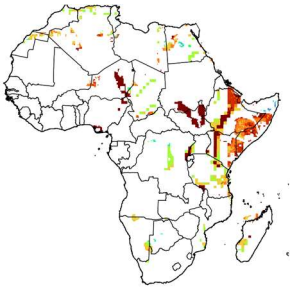

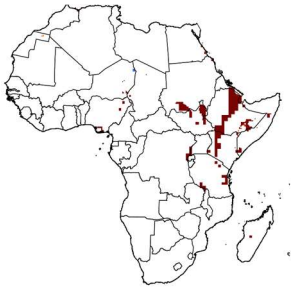

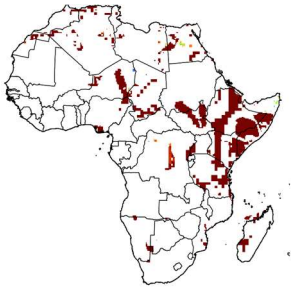

DP

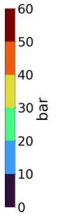

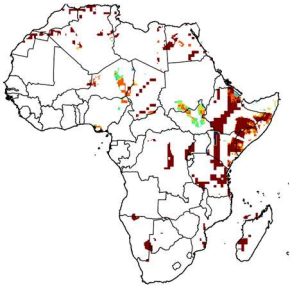

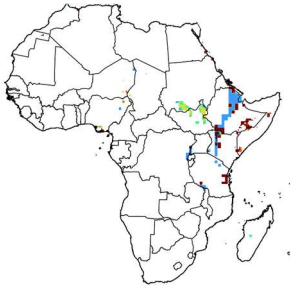

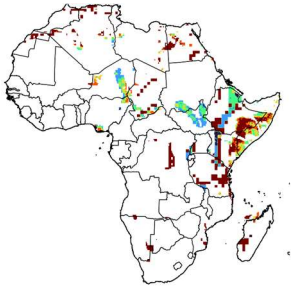

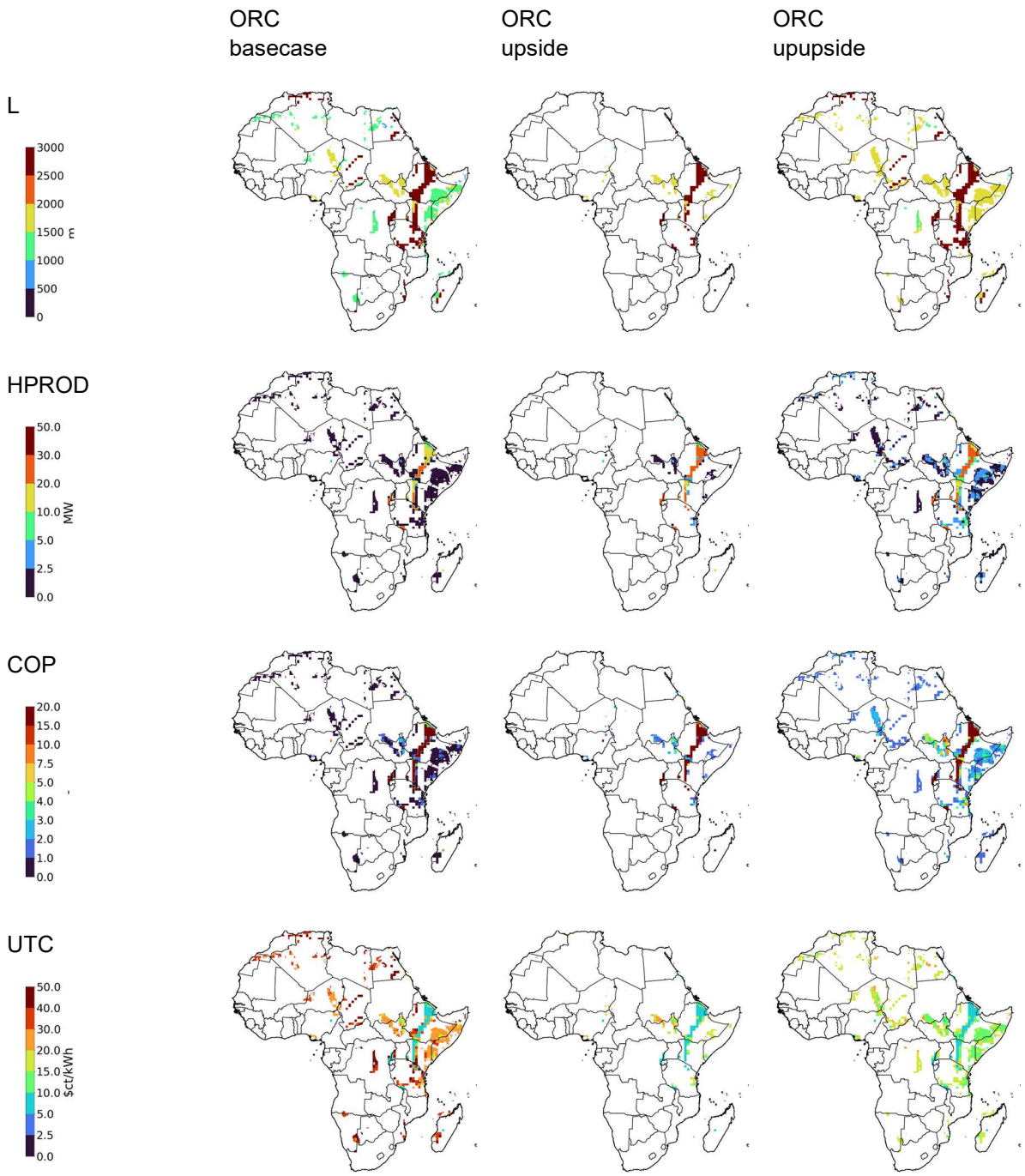

Figure 16 key performance parameters for ORC

5 Socio economic Indicator maps

Subsequently , the resulting maps have been blended to compound index maps as follows

INDEX value	LCOE cutoff [US$cts/kWh] directheat/other	Scenario considered	Permeability Pvalue	Geothermal gradient scale
10	>=10/20	upupside	25	1.3
20	<10/20	upupside	25	1.3
30	<10/20	Upside	25	1
40	<5/10	Basecase	50	1
50	<2.5/5	basecase	50	1

Table 9 index values for indicator maps displayed in Figure 17

Geothermal energy conversion	Direct heat	Direct Heat HP	Chill	ORC
roads	<50 km	<50 km	<50 km	<50 km
Population density	>20/km2	>20/km2	20/km2	
temperature			>20	

Table 10 filters applied for different indicator maps displayed in in Figure 17

Figure 17 (next pages) indicator maps of energy conversion scenarios in accordance to base case, upside and upupside scenarios as defined in section 2 and in agreement with indexation following Table 9 (left column) and filtering according to Table 10

directheat

directheat filtered

UTC_INDEX

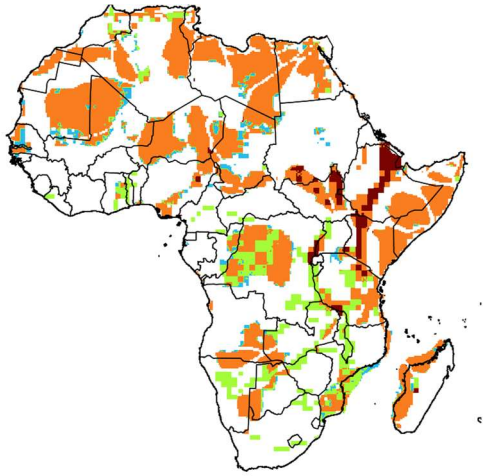

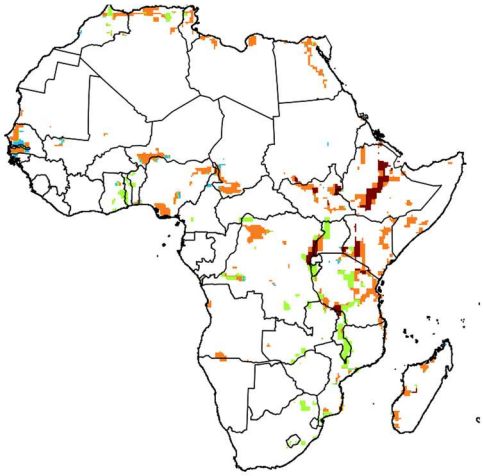

directheatHP

directheatHP filtered

UTC_INDEX

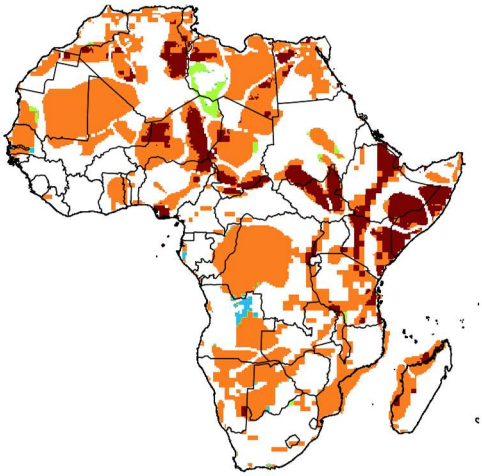

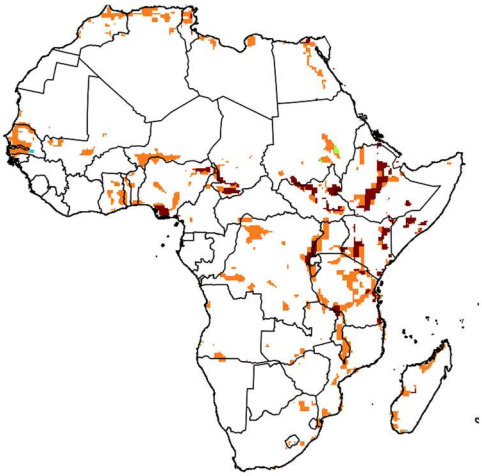

chiller

chiller filtered

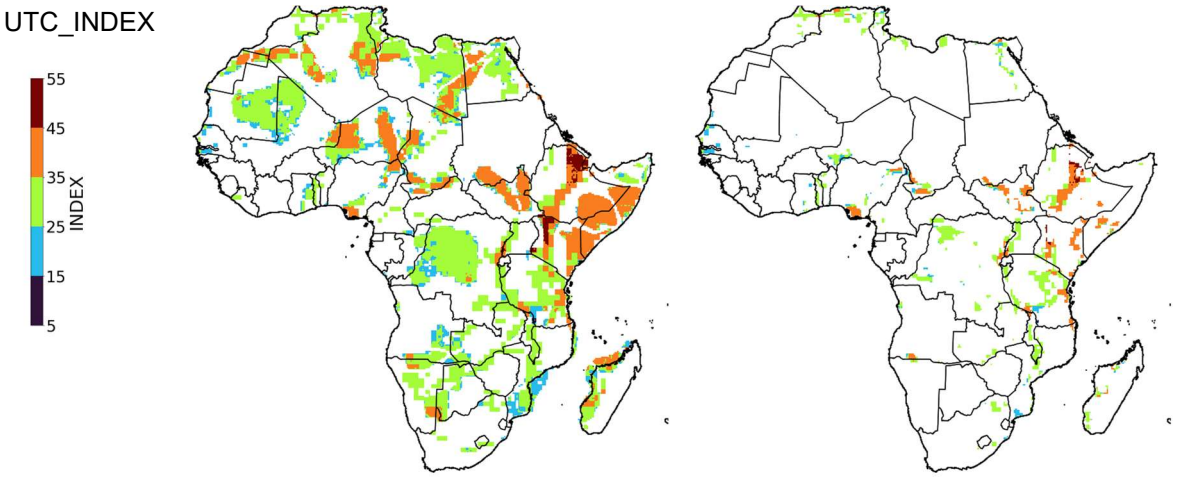

ORC

ORC filtered

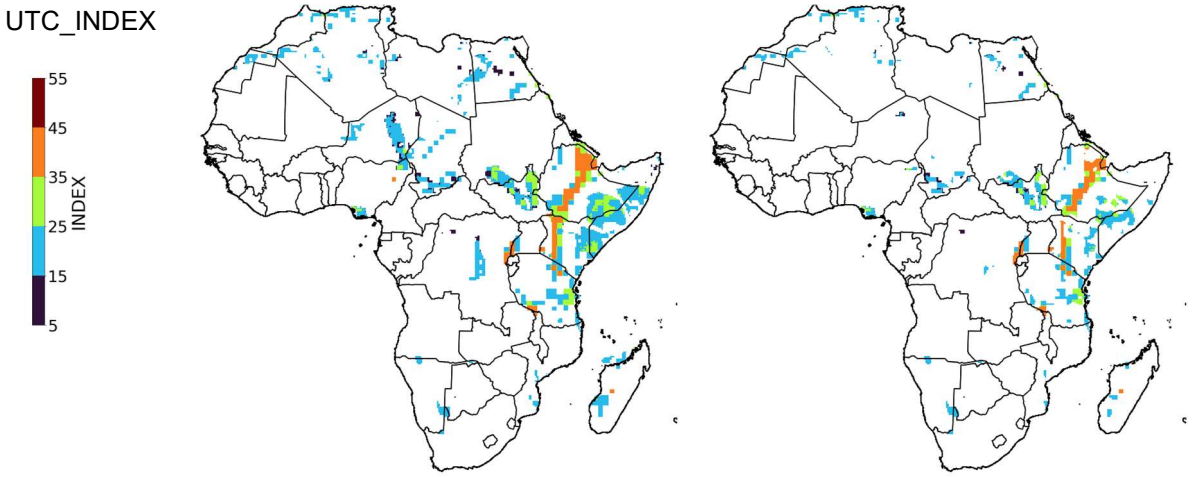

6 References

Auld, A., Hogg, S., Berson, A., Cluyas, J., 2014. Power production via North Sea Hot Brines. Energy, 78, https://doi.org/10.1016/j.energy.2014.10.056

Ayou, D., Coronas, A., 2020. New Developments and Progress in Absorption Chillers for Solar Cooling Applications. Applied sciences, 10, 4073; doi:10.3390/app10124073.

Békési E., Struijk, M., Bonté, D., Veldkamp, J.G., Limberger, J., Fokker, P.A., Vrijlandt, M. & van Wees, J.D. (2020). An updated geothermal model of the Dutch subsurface based on inversion of temperature data. Geothermics 88(11). doi: 10.1016/j.geothermics.2020.101880

Bonté D., van Wees J.-D. & Verweij J.M. (2012). Subsurface temperature of the onshore Netherlands: new temperature dataset and modelling. Netherlands Journal of Geosciences — Geologie en Mijnbouw, 91–4, 491-515, 2012.

Choudbury, A., Chatterjee, P.K., Sarkar., J.P., 2010. Review paper on solar-powered air-conditioning through adsorption route. Renewable and Sustainable Energy Reviews 14 (2010) 2189–2195

DOE, 2017. U.S. Department of Energy factsheet Combined heat and power. Technology fact sheet series, https://www.energy.gov/eere/amo/downloads/absorption-chillers-chp-systems-doe-chp-technology-fact-sheet-series-fact-sheet

El-Sharkawi, I., AbdelMeguid, H., Saha, B.B., 2014. Potential application of solar powered adsorption cooling systems in the Middle East., http://dx.doi.org/10.1016/j.apenergy.2014.03.092.

Frick, S., Kaltschmitt, M., Schröder, G., Life cycle assessment of geothermal binary power plants using enhanced low-temperature reservoirs. *Energy,* (2010), 35, 2281-2294.

Hantschel, T. and Kauerauf, A.I. (2009). Fundamentals of basin and petroleum systems modeling. Springer Berlin, Heidelberg. 476p, doi: https://doi.org/10.1007/978-3-540-72318-9

Holmes et al., 2021; Multilateral-closed-loop-geothermal-systems-as-a-ZELFR.pdf (eavor.com)

Moon, H., Sarrouk, S.J., 2012. Efficiency of geothermal power plants: a worldwide review. New Zealand Gooethermal Workshop 2012 Proceedings.

Pluymaekers, M., Kramers, L., Van Wees, J. D., Kronimus, A., Nelskamp, S., Boxem, T., & Bonté, D., 2012. Reservoir characterisation of aquifers for direct heat production: Methodology and screening of the potential reservoirs for the Netherlands. Netherlands Journal of Geosciences 91 (04): 621-636.

Van Wees, 2021. Audit Report Eavor Loop. TNO - Eavor-Loop™ Audit Report - Eavor

Van Wees, J.D., Kronimus, A., Van Putten, M., Pluymaekers, M., Mijnlieff, H., Van Hoof, P., Obdam, A. and Kramers, L.: Geothermal aquifer performance assessment for direct heat production – Methodology and application to Rotliegend aquifers, Netherlands Journal of Geosciences, (2012) 91-4, 651-665

Vrijlandt, M.A.W., Struijk E.L.M., Brunner L.G., Veldkamp J.G., Witmans N., Maljers D., Van Wees J.D., 2021. ThermoGIS: from a Static to a Dynamic approach for National Geothermal Resource Information and Development, World Geothermal Congress 2020. https://www.geothermal-energy.org/pdf/IGAstandard/WGC/2020/16071.pdf